Nanoscale

ROYAL SOCIETY OF CHEMISTRY

PAPER

View Article Online
View Journal | View Issue

Cite this: *Nanoscale*, 2023, **15**, 15831

A magnetic field-driven multi-functional "medical ship" for intestinal tissue collection *in vivo*†

Junmin Liu,‡[a] Zhiyuan Huang,‡[a] Honger Yue,[a] Rencheng Zhuang,[a] Longqiu Li,[a] Xiaocong Chang*[a,b] and Dekai Zhou*[a,b]

The incidence of intestinal cancer has risen significantly. Because of the many challenges posed by the complex environment of the intestine, it is difficult to diagnose accurately and painlessly using conventional methods, which requires the development of new body-friendly diagnostic methods. Micro- and nanomotors show great potential for biomedical applications in restricted environments. However, the difficulty of recycling has been a constraint in the collection of biological tissues for diagnostic purposes. Here, we propose a multi-functional "medical ship" (MFMS) that can be rapidly driven by a magnetic field and can reversibly "open" and "close" its internal storage space under NIR laser irradiation. It provides a transportation and recovery platform for micro- and nanomotors and cargoes. In addition, fast selection of the MFMS and magnetic nanoparticles (MNPs) can be realized through adjusting the strength and frequency of the external magnetic field. Rapid encapsulation of intestinal tissues by MNPs was achieved using a low-frequency rotating magnetic field. In addition, we demonstrated the controlled release of MNPs using the MFMS and the collection of intestinal tissues. The proposed MFMS is an intelligent and controllable transportation platform with a simple structure, which is expected to be a new tool for performing medical tasks within the digestive system.

Received 31st July 2023,
Accepted 7th September 2023

DOI: 10.1039/d3nr03770c

rsc.li/nanoscale

1. Introduction

The incidence of intestinal cancer, particularly small intestinal cancer, has risen significantly in recent years.[1] However, the complex intestinal environment presents a challenge in the diagnosis of intestinal cancer. Currently, various traditional diagnostic methods, such as endoscopy and computed tomography, are used to diagnose intestinal cancer.[2–4] However, these methods face significant challenges due to their limitations such as high invasiveness, susceptibility to damage to the intestinal mucosa and low accuracy. Therefore, it is important to develop new methods for diagnosing intestinal cancer.

Recently, micro- and nanomotors have been receiving a lot of attention for their multiple propulsion mechanisms, and their potential to navigate in complex constrained environments.[5] In particular, they have potential applications in revolutionize biomedical diagnostics, minimally invasive surgery, and targeted drug delivery, due to their ability to reach inaccessible areas in the human body in a minimally or non-invasive fashion for diagnostic and therapeutic purposes.[6–18] Micro- and nanomotors can be driven by chemical,[19–21] electric,[22,23] ultrasonic,[24–26] magnetic and optical fields.[27–33] Among them, magnetic field-driven micro- and nanomotors have the advantages of strong controllability, non-invasiveness and low hazard.[34–38] In particular, the magnetic field exhibits superior performance in the synergistic operation of micro- and nanomotors. For example, by applying a time-varying magnetic field, clusters of magnetic micro-disks can be controlled to collaboratively transport goods in a reconfigurable manner.[39] Magnetic field-driven micro- and nanomotors offer the opportunity to accurately and painlessly diagnose and treat intestinal cancer. However, due to the small size of micro- and nanomotors, the collected cancer cells or tissues cannot be effectively recycled. Therefore, we need a novel platform that can preserve the collected cancer cells or tissues during the process of transportation and recycling based on micro- and nanomotors. Most importantly, the platform needs to provide closed or open storage for micro- and nanomotors and cargoes in a controlled manner. This strategy will greatly expand the functionality of micro- and nanomotors. Smart materials are functional materials that perform operations in response to external stimuli (*e.g.* pH, light, heat). For example, micromotors that utilize the ion-sensitivity of alginate hydrogels enable

[a]*State Key Laboratory of Robotics and System, Harbin Institute of Technology, Harbin, Heilongjiang 150001, China. E-mail: xiaocong@hit.edu.cn, dekaizhou@hit.edu.cn*
[b]*Chongqing Research Institute of Harbin Institute of Technology, Chongqing, 400722, China*

†Electronic supplementary information (ESI) available. See DOI: https://doi.org/10.1039/d3nr03770c

‡The authors contributed equally to this work.

the release and gripping of cargoes.[40] Thus, we believe that smart materials can provide insights into building controlled platforms whose storage space can be turned "open" or "closed" on demand in response to external stimuli.

In this study, based on the reversible deformation of temperature-controlled smart materials, we report a simple method to construct a multi-functional "medical ship" (MFMS) with a cabin whose "opening" or "closing" can be controlled.

With magnetically responsive wheels as the "drive unit" and a shape memory alloy spring as the "deformation unit", the MFMS can overcome the high adhesive force of the inner wall of the intestine to move under a magnetic field, and can be controlled to "open" or "close" the cabin under near-infrared (NIR) laser irradiation. By varying the magnetic field pattern and frequency, the magnetic nanoparticles (MNPs) carried inside it can reversibly switch between dense disk-like clusters (motility) and dispersed rod-like clusters (adsorption), enabling the capture and transport of intestinal tissues at specific locations. Notably, the control object can be selected controllably by changing the magnetic field frequency and intensity. Our experimental results suggest that the integration of the MFMS with MNPs provides a simple and efficient new strategy for the harvesting of intestinal cells. Fig. 1 shows a schematic diagram of the MFMS carrying MNPs to collect tissues in the intestine. In the intestine, the MFMS releases MNPs, which move through a magnetic field to collect intestinal cells, after which the cells are transported back to the MFMS for preservation.

2. Experimental section

2.1. Materials and characterization

CN981 NS was purchased from Shkingchem Inc. Tripropylene glycol diacrylate (TPGDA) was purchased from Curease Chemical Inc. Poly (ethylene glycol) diacrylate (PEGDA) was purchased from Sigma-Aldrich Inc. Irgacure 819 was purchased from BASF Inc. NdFeB microparticles and Fe_3O_4 nanoparticles (NPs) were purchased from Shanghai Naiou Nano technology Inc. $FeCl_3{\cdot}6H_2O$, sodium acetate and polyethylene glycol were purchased from Shanghai Aladdin Biochemical Technology Co., Ltd. Shape memory alloy springs were purchased from Suzhou Xinghai Electronic Commerce Co., Ltd. The morphology of chicken intestinal tissue encapsulated by magnetic nanoparticles was investigated using scanning electron microscopy (Thermo Scientific Scios 2 DualBeam) and imaged and chemically mapped using an Xplore energy dispersive spectrometer (Oxford Instruments).

2.2. Preparation of the MFMS

The MFMS consists of two magnetically responsive wheels and a shape memory alloy spring. Magnetically responsive wheels for the MFMS were prepared from magnetic photosensitive resins using a homemade μCLIP system. The preparation process of magnetic photosensitive resins has been reported in our previous work.[41] Briefly, the magnetic photosensitive resin was based on three monomers, including the CN981 NS monomer, TPGDA and PEGDA. CN981 NS and TPGDA were mixed in a 4 : 1 (w/w) ratio using a magnetic stirrer for 2 h at 50 °C and 400 rpm. They were then mixed with PEGDA in a 5 : 3 (w/w) ratio under the same mixing conditions. Then 2 wt% of Irgacure 819 as a photoinitiator was added to this mixture and sonicated for 2 h. Finally, 20 wt% of magnetic particles as a ferromagnetic additive was added to the mixture. The magnetic particles consisted of NdFeB particles (1–2 μm) and Fe_3O_4 nanoparticles (10 nm) mixed in a 1 : 1 (w/w) ratio. The mixture was mixed in ultrasonic for 2 h, mechanical stirring for 15 min and vacuum for 30 min to get the final magnetic photosensitive resin. The homemade μCLIP system has been illustrated in our previous work.[42] It provides micron-level spatial resolution and a millimetre-level building area for the preparation of the MFMS. The printed MFMS was sequentially subjected to a 2 min acetone soak, a 5 min ultrasonic clean (in ethanol solution), and a 30 min drying periodfollowed by 10 min of post-curing under UV light (405 nm), resulting in a magnetically responsive wheel. Finally, the

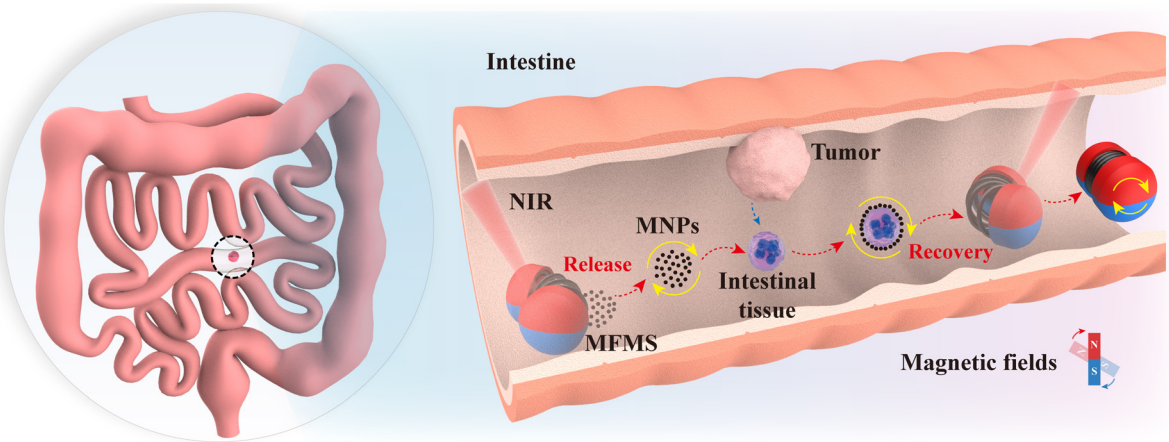

Fig. 1 Schematic illustration of the MFMS carrying MNPs to collect tissues in the intestine.

MFMS was obtained after assembling the magnetically responsive wheels and shape memory alloy springs together using a light-curing adhesive.

2.3. Preparation of Fe_3O_4 nanoparticles

Fe_3O_4 NPs were synthesized according to a previously reported hydrothermal method.[43] Briefly, a mixed solution of $FeCl_3.6H_2O$ (2.7 g), ethylene glycol (80 mL), sodium acetate (7.2 g), and polyethylene glycol (2.0 g) was magnetically stirred for 30 min before being transferred and sealed in a Teflon-lined autoclave (100 mL capacity). The autoclave was kept at 200 °C for 12 h and then cooled naturally to room temperature. The product was collected and washed five times with deionized water and ethanol, and then dried at 60 °C for 6 h.

2.4. Experimental setup and systems

The magnetic field was generated using a homemade three-dimensional Helmholtz coil magnetron system. The magnetron system provides a uniform AC magnetic field in any direction with a frequency of between 0 and 60 Hz, and an effective space of the uniform field of 5 cm × 7 cm × 3 cm. The magnetron system can be used in conjunction with an Olympus inverted (IX73) stereomicroscope (Phenix, XTL-165-VT), and utilizes a CCD camera (FLIR-GS3-U3-51S5C-C) to capture and record the movement of the MFMS and magnetic NPs. A 500 mW near infrared laser (Shenzhen Infrared Laser Technology Co., Ltd, HW808AD500-16GD) was used to provide the heat needed to open the compartment on the MFMS. ImageJ (National Institutes of Health, NIH) was used for data processing.

3. Results and discussion

3.1. Motion behavior of the MFMS

Inspired by medical ships at sea, for the painless diagnosis of intestinal cancer, we proposed a magnetically driven MFMS that can collect tissues in the intestinal environment, which was filled with mucus and folds. The MFMS has a diameter of 5.5 mm and a length of 6.3 mm, which is 1/4 of the average diameter of the human small intestine (2.5 cm). It consists of two parts, a magnetically responsive wheel as the "drive unit" and a shape memory alloy spring as the "deformation unit" (Fig. 2(a)). Magnetically responsive wheels were fabricated utilizing a homemade μCLIP system. The resin material used was doped with NdFeB microparticles and Fe_3O_4 NPs (1 : 1 w/w) (Fig. S1†). NdFeB microparticles significantly increased the residual magnetism of the fabricated magnetically responsive wheels (Fig. S2†). This provides the basis for high responsiveness and high controllability of the MFMS in the magnetic field after magnetization. A customized spring was made of a two-way shape memory alloy. It had an outer diameter of 5 mm, an inner diameter of 4 mm and a wire diameter of 0.5 mm. When assembled with the magnetically responsive wheels, its outer diameter has a height of 0.25 mm from the bottom surface. In addition, it will stretch at higher than 50 °C and return to a dense state at lower than 40 °C. This ensures that the MFMS does not open uncontrollably in the intestine, but also allows it to perform its tasks within the body's tolerable range (the normal temperature of the intestine is 36.5–37.7 °C). Depending on the magnetic responsiveness of the "drive unit", the MFMS can controllably move under an external rolling magnetic field $\boldsymbol{H}(t) = H_0(A\cos(2\pi ft)\boldsymbol{e}_x + B\cos(2\pi ft)\boldsymbol{e}_y + \sin(2\pi ft)\boldsymbol{e}_z)$ (where $\boldsymbol{H}$ is the magnetic field strength, H_0 is the amplitude, f is the frequency, A and B are variables and $\sqrt{A^2 + B^2} = 1$), which is a rotating magnetic field perpendicular to the bottom surface (*e.g.* $\boldsymbol{H}_{XZ}$ denotes a counterclockwise rolling magnetic field in the X–Z plane), and has the ability to cross barriers. Depending on the temperature-controlled reversible deformation capability of the "deformation unit", the MFMS can control the "opening" or "closing" of its cabin under NIR laser irradiation (Fig. 2(b)). Using a homemade 3D Helmholtz coil magnetron system (Fig. S3†), we conducted navigation experiments in a 3D printed S-channel to evaluate the mobility and controllability of the MFMS in a complex environment. Fig. 2(c) shows that the MFMS allows precise directional control in the S-channel (Video S1†). Although the cylindrical shape has an effect on its ability to turn, this can be solved by positional adjustment of it using an external magnetic field. In addition, we performed deformation experiments of the MFMS on slides to assess the controllability and reversibility of the "opening" and "closing" of its cabin. Fig. 2(d) shows that the MFMS can reversibly open and close its cabin under NIR laser irradiation (Video S2†). It is worth noting that the "open" direction of the MFMS cabin tends to be the opposite side of the NIR laser focus. This is explainable due to the localized stretching of the shape memory alloy. This feature would facilitate the controlled release of MNPs or the receipt of cargo by the MFMS.

In order to collect tissues or cells from the intestine, the MFMS must break through the acidic environment of the stomach. Therefore, we also performed acid corrosion experiments on the MFMS (Fig. 2(e)). The experimental results showed that the morphology and structure of the MFMS remained unchanged after 5 h of immersion in an acidic solution at pH = 1. Moreover, its motility and deformation properties were not affected. In addition, to investigate the motility of the MFMS in the highly viscous environment of the intestine, we analyzed the effects of the strength and frequency of the magnetic field as well as the viscosity of the environment on the velocity of the MFMS. As shown in Fig. 2(f), the velocity of the MFMS increases with increasing magnetic field strength. More specifically, the peak velocity of the MFMS increases from 82.2 mm s^{-1} to 138.8 mm s^{-1} as the field strength increases from 1 mT to 5 mT. In addition, in the magnetic field frequency range of 5 Hz–60 Hz, there exists a peak frequency corresponding to the peak velocity. The velocity trend of the MFMS changes at the peak frequency. This is due to the frequency hysteresis in the rolling motion of the MFMS. It is worth noting that at certain frequencies, the MFMS cannot move. This is due to the fact that the magnetic torque imparted to the MFMS by the high-frequency magnetic field is

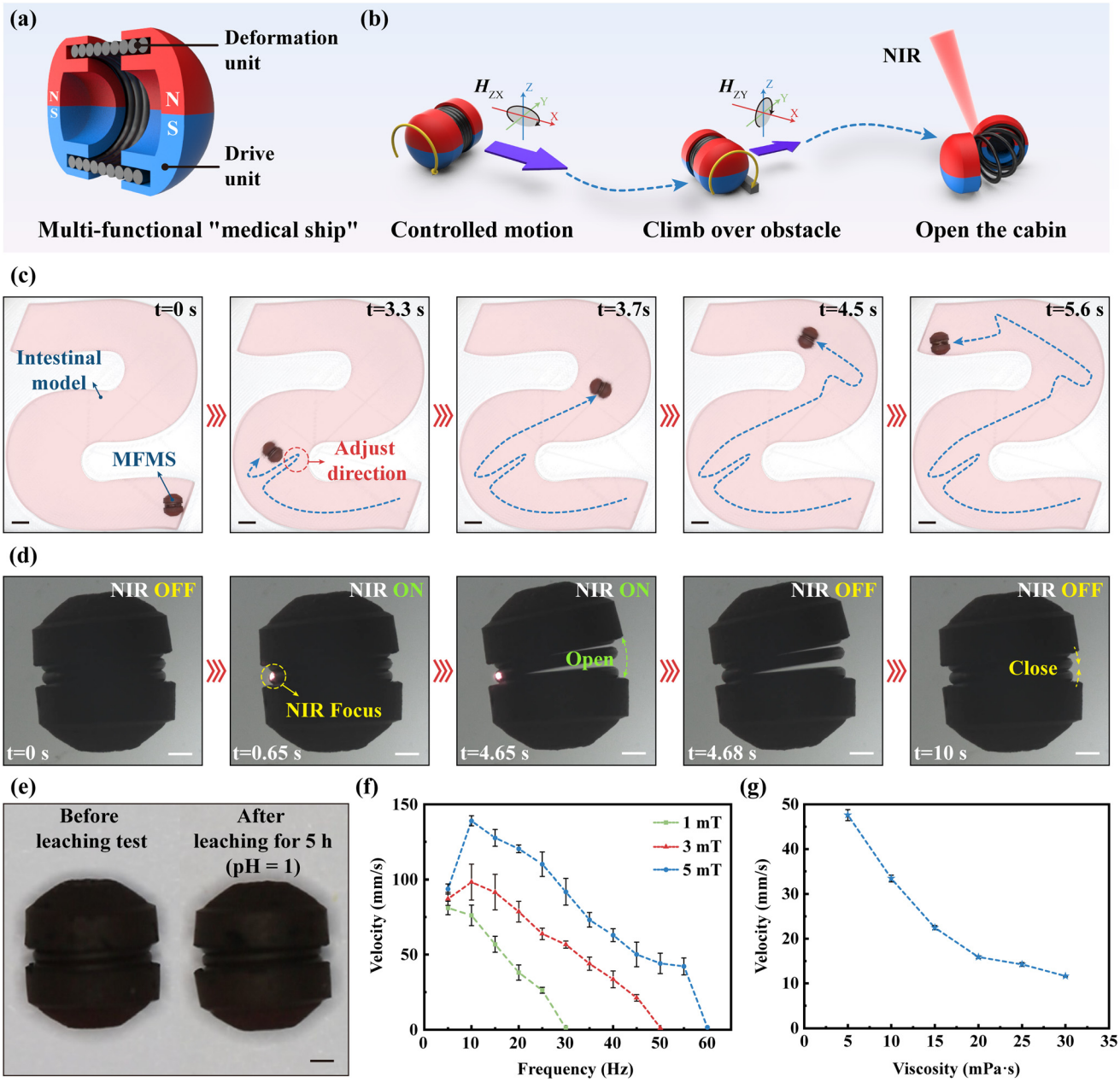

Fig. 2 Motion behavior of the MFMS. (a) Schematic illustration of the components of the MFMS. (b) Schematic illustration of MFMS motion and obstacle crossing in a magnetic field, and "opening" of the cabin under NIR laser irradiation. (c) Navigating experiment of the MFMS in an S-channel. (d) Reversible "opening" and "closing" of the cabin of the MFMS under NIR laser irradiation. (e) Image comparison of the MFMS before and after 5 h immersion in an acidic solution at pH 1. (f) Velocity variation of the MFMS at different magnetic field strengths and frequencies. (g) Velocity variation of the MFMS in medium environments with different viscosities. Scale bars in (c) are 5 mm, and in (d) and (e) are 1 mm.

not sufficient to overcome its friction with the bottom surface. Moreover, this cut-off frequency (corresponding to the initial frequency at which no motion is possible) increases with field strength. This is because the magnetic torque of the MFMS increases with field strength. Also, this is the reason why the peak frequency increases with increasing field strength. As shown in Fig. 2(g), the velocity of the MFMS decreases with increasing ambient viscosity of the medium (a magnetic field frequency of 10 Hz and a strength of 5 mT). This is due to the increase in viscosity, which leads to an increase in drag on the MFMS. However, the MFMS was able to maintain a motion velocity of 11.6 mm s^{-1} in a medium environment with a viscosity of 30 mPa s. Predictably, the MFMS still has the ability to move quickly in the intestine (intestinal fluid viscosity 23.4 ± 8.2 mPa s).

3.2. Cluster motion behavior of MNPs

As the actuators of the collected intestinal tissues or cells carried by the MFMS, the motion behavior of MNPs will

directly affect the efficiency of performing the task. Fig. 3(a) illustrates the clustering of MNPs into a dense disc. In the initial state, MNPs were randomly and very loosely distributed on the substrate. Upon application of a rotating magnetic field parallel to the bottom surface, the MNPs aggregate into loosely and irregularly packed clusters under the competition between the magnetic dipole interaction and the hydrodynamic drag. We simulated the magnetic field distribution around the MNPs in the magnetic field (Fig. 3(c)). The results show that the magnetization direction of the MNPs is aligned with the direction of the external magnetic field and an interconnected magnetic field is generated between the MNPs. This attraction between magnetic dipoles will drive the MNPs to aggregate with each other. In order to produce directional motion in the clusters of MNPs, the magnetic field was converted to a rolling magnetic field. During this process, the loose and irregular clusters that had gathered were immediately rotated by 90° in response to the change in the magnetic field and advanced in

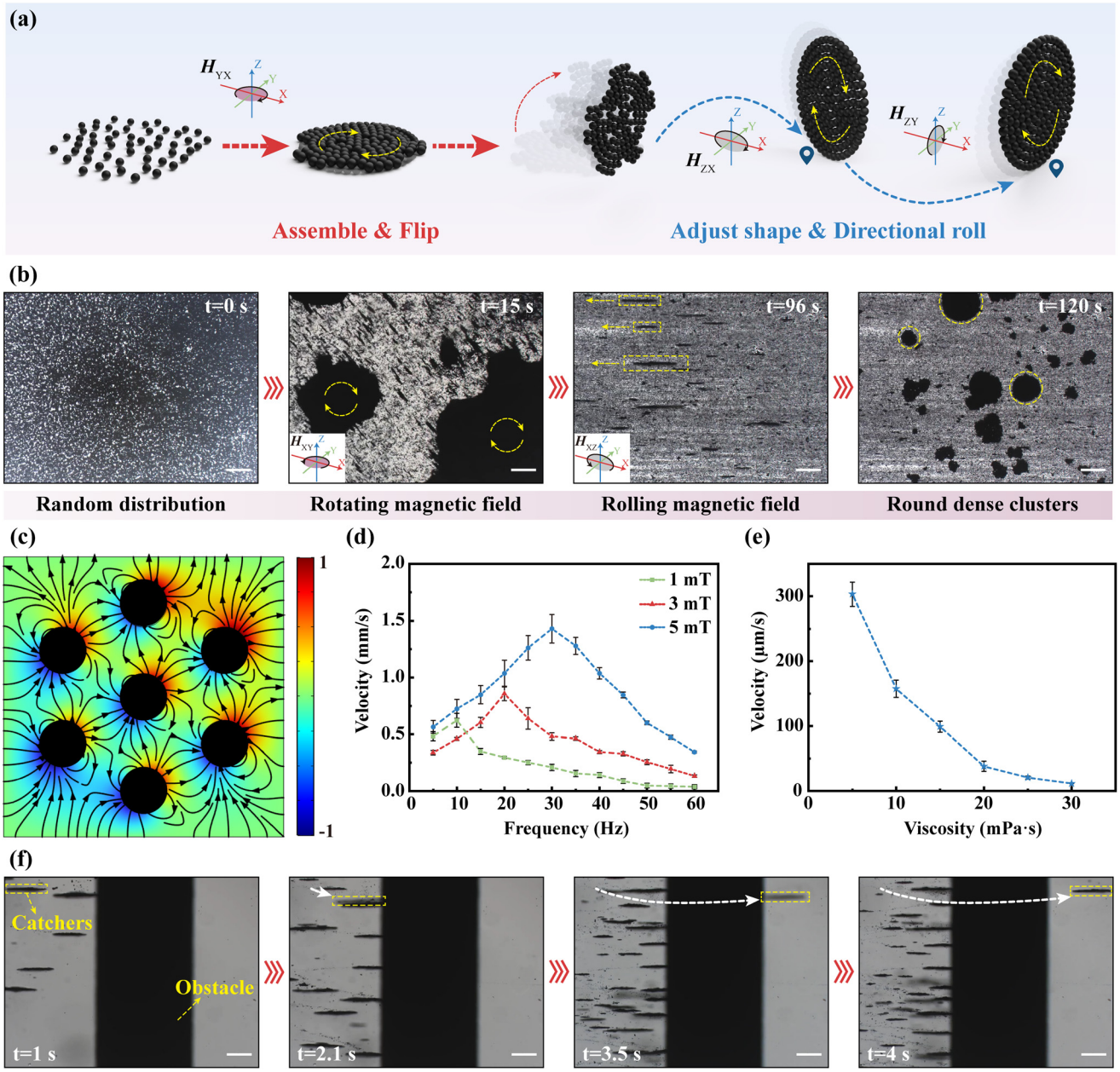

Fig. 3 Cluster motion behavior of MNPs. (a) Schematic illustration of the magnetron clustering process of MNPs. (b) Time-lapse snapshots of the magnetron clustering process in MNPs. (c) Simulation of magnetic field distribution in MNPs. (d) Velocity variation of the clusters of MNPs at different magnetic field strengths and frequencies. (e) Velocity variation of the clusters of MNPs in medium environments with different viscosities. (f) Time-lapse snapshots of the clusters of MNPs climbing over an obstacle. Scale bars in (b) and (f) are 200 μm.

a rolling fashion along the plane of the rotating magnetic field. Therefore, the direction of the clusters of MNPs can be conveniently controlled by controlling the working plane of the external rolling magnetic field. Moreover, during the rolling process, clusters of MNPs change from a loose irregular structure to a dense and regular circular shape, due to the fact that the edges of clusters are cyclically subjected to a contact force perpendicular to the bottom surface. We also experimentally verified the formation of disk-like structures using MNPs (Fig. 3(b), Video S3†). It is worth noting that loose clusters formed under a rotating magnetic field will break up into small clusters when the external magnetic field changes to a rolling magnetic field. This is due to the fact that the magnetic dipole interaction between the MNPs is not sufficient to overcome the resistance due to the instantaneous change when the plane of magnetic field action is suddenly changed. To assess the mobility of the clusters of MNPs in the intestine, we analyzed the effects of the strength and frequency of the magnetic field, as well as the viscosity of the environment, on the velocity of clusters. As shown in Fig. 3(d), like MFMS, the velocity of the MNP clusters increases with a field strength of up to 1.4 mm s^{-1}. Moreover, the clusters of MNPs also suffer from frequency hysteresis and therefore peak frequencies. Similarly, the peak frequency of the MNP clusters increases as the field strength increases. In addition, clusters of MNPs were motile in both the measured field strength and frequency range. This is due to the fact that the clusters of MNPs were subjected to much less resistance than the MFMS, which had to overcome friction with the bottom surface, and therefore the magnetic torque applied to them was sufficient to set them in motion. This different frequency response will help us to select the control object by controlling the frequency of the external magnetic field. In addition, as with the MFMS, the velocity of the clusters of MNPs decreases as the viscosity of the medium environment increases (Fig. 3(e)). Moreover, even in a highly viscous environment of 30 mPa s, it still had a speed of 11.4 μm s^{-1}, showing a strong ability to overcome the highly viscous environment of the intestinal tract. In addition, we performed barrier-crossing experiments with the clusters of MNPs to assess their maneuverability in the complex environment of the intestine and into the MFMS. Fig. 3(f) shows a time-lapse snapshot of a cluster of MNPs being controlled to climb over a cylindrical obstacle with a diameter of 785 μm (Video S4†). When a cluster of MNPs comes into contact with a cylindrical obstacle, the cluster is subjected to a friction force along the tangential direction of the point of contact in the opposite direction to the linear velocity of its edges, and

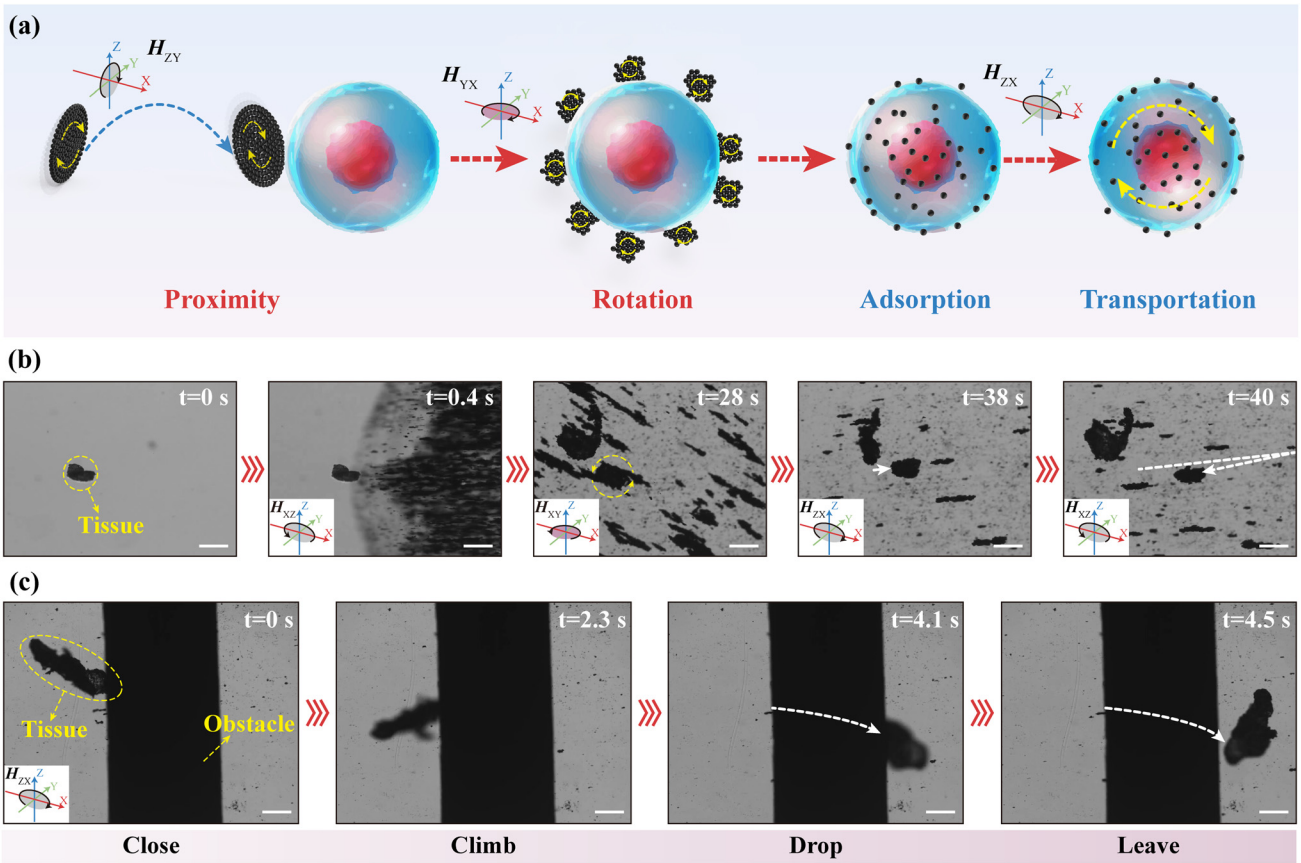

Fig. 4 Clusters of MNPs transport intestinal tissues. (a) Schematic illustration of the clusters of MNPs to transport intestinal tissues. (b) Time-lapse snapshots of the clusters of MNPs to transport intestinal tissues. (c) Time-lapse snapshots of intestinal tissues encapsulated by MNPs climbing over an obstacle. Scale bars in (b) and (c) are 200 μm.

under the action of this force, the cluster is equipped with the ability to go over the obstacle.

3.3. Clusters of MNPs transport intestinal tissues

We performed experiments to assess the controllability of the clusters of MNPs to transport intestinal tissues. Fig. 4(a) shows the process by which the clusters of MNPs transport intestinal tissues. First, they approached the intestinal tissues under a rolling magnetic field and dispersed into small clusters under a low-frequency rotating magnetic field. The size of the cluster is determined by the Mason number:[44]

$$\mathrm{Ma} \equiv \frac{12^2 \mu_0 \eta \omega}{M^2}$$

where M is the magnetization of a MNP, μ_0 is the vacuum magnetic permeability, η is the viscosity of the medium environment, and ω is the angular velocity of the external rotating magnetic field. When the frequency of the external magnetic field is high, it is easy to form large nearly solidified isotropic circular clusters. In addition, the shape of the clusters is also correlated with the Brownian relaxation time of the MNPs. It is defined as follows:[44]

$$\tau_B \equiv \frac{3\pi\eta R^3}{kT}$$

where R is the radius of a MNP, k is the Boltzmann constant, and T is the temperature of the medium environment. When the angular velocity of the magnetic field rotation is lower than the translational motion of the MNPs, the MNPs are more likely to form rod-like clusters rather than isotropic circular clusters. In our experiments, the critical frequency for cluster shape change is 15.8 Hz. We simulated the motion of the clusters of MNPs under a low-frequency rotating magnetic field to better understand how the clusters deform. The results showed that the clusters of MNPs do not simply elongate outward, but first diffuse outward as a whole, then extrude inward along the short axis and lengthen along the long axis (Fig. S4†). As these small clusters rotate around the intestinal tissue, they cause some of the MNPs to adsorb to the surface of the intestinal tissue due to adhesive forces with the biological tissue, which is the basis for the intestinal tissue to be driven by the magnetic field (Fig. S5†). Moreover, rod-like clusters have a greater rotational velocity than isotropic circular clusters. Therefore, the low-frequency rotating magnetic field is more suitable for MNPs to contact with intestinal tissues, thus increasing the adsorption probability. When enough MNPs have been adsorbed on the surface of the intestinal tissues, the intestinal tissues will be driven by an external magnetic field and exhibit strong motility. Fig. 4(b) shows the time-lapse snapshots of the clusters of MNPs transporting intestinal tissues, demonstrating that clusters of MNPs can easily endow intestinal tissues with magnetic responsiveness for controlled motion under magnetic fields (Video S5†). In addition, we performed barrier-crossing experiments with

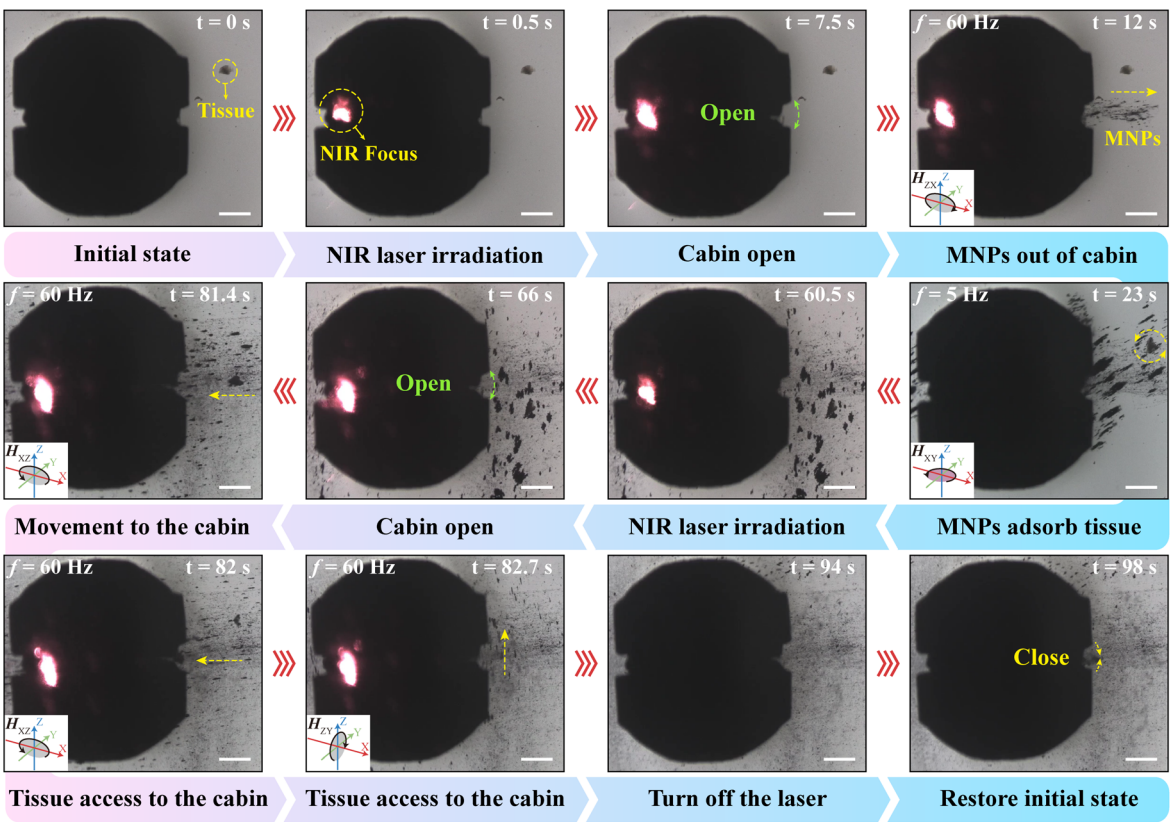

Fig. 5 Intestinal tissues collected by the MFMS carrying MNPs. Scale bars: 1 mm.

intestinal tissues encapsulated by MNPs to assess their maneuverability. Fig. 4(c) shows a time-lapse snapshot of the intestinal tissue encapsulated by MNPs being controlled to climb over a cylindrical obstacle with a diameter of 785 μm (Video S6†). This obstacle is higher than the height (750 μm) of the inner surface of the cabin of the MFMS from the bottom. Therefore, the intestinal tissue encapsulated by the MNPs has the ability to enter the cabin of the MFMS. Although the irregular shape of the intestinal tissue increased its difficulty in being driven, the friction still gives it the ability to go over obstacles when it comes in contact with them.

3.4. Controlled intestinal tissue collection

We experimentally verified the feasibility of the MFMS to release MNPs for collecting intestinal tissues (Fig. 5, Video S7†). First, for ease of observation, the MFMS with MNP solution was placed with the intestinal tissue in an area where it could be observed using a microscope. Then, NIR laser irradiation was applied to one side of the shape-memory alloy spring of the MFMS at 0.5 s. After 7 s the cabin of the MFMS was opened, and thereupon we applied a rolling magnetic field with a strength of 5 mT and a frequency of 60 Hz to control the MNPs out of the cabin of the MFMS. At this magnetic field parameter, the MFMS was not motile. Moreover, during the above process, the MNPs only came out of the opening of the cabin of the MFMS, which shows the excellent sealing of the MFMS. We controlled the movement of the clusters of MNPs towards the vicinity of intestinal tissues by changing the working plane of the external rolling magnetic field. Subsequently, the magnetic field was transformed into a rotating magnetic field with a frequency of 5 Hz to achieve efficient wrapping of the MNPs around the intestinal tissues. After effective control of the intestinal tissue was achieved, the magnetic field was turned off and an NIR laser was applied to irradiate one side of the MFMS. After its cabin was opened, a rolling magnetic field was applied to control the intestinal tissue into the MFMS. Finally, the laser and magnetic field were turned off to restore the MFMS to its initial state. In summary, we demonstrated that the MFMS can release MNPs in a controlled manner and utilize MNPs for intestinal tissue capture, thus successfully collecting intestinal tissues.

4. Conclusions

We present a magnetically driven MFMS that imitates a medical ship at sea for accurate and painless collection of intestinal tissues for intestinal cancer diagnosis in complex intestinal tracts with highly viscous medium environments. The two-way shape-memory alloy spring acts as a "deformation unit" that allows the MFMS to controllably "open" and "close" its cabin under NIR laser irradiation. A magnetically responsive wheel based on a resin material doped with hard magnetic NdFeB microparticles acts as a "drive unit" to enable the MFMS to move in a highly viscous environment under an external alternating magnetic field. The results showed that it had a velocity of 11.6 mm s^{-1} even in an environment with a viscosity of 30 mPa s. This is difficult to achieve for micro- and nanomotors. Therefore, this MFMS also offers the possibility for micro- and nanomotors to reach a specified position quickly. In addition, we investigated the motion behavior of MNPs carried by the MFMS. They can form dense disk-like clusters under an external magnetic field. The disk-like cluster has the ability to move controllably in highly viscous environments, as well as the ability to go over obstacles that are ten times its diameter. In addition, we investigated the effects of field strength and frequency on the velocity of the MFMS and clusters of MNPs. The experimental results showed that the controlled objects can be conveniently selected by changing the field strength and frequency. In addition, the high-speed rotation characteristics of the rod-like clusters of MNPs under a low-frequency rotating magnetic field were utilized so that the MNPs could be rapidly adsorbed onto the surface of intestinal tissues, which in turn enabled the transport of intestinal tissues under a rolling magnetic field. The experimental results showed that the MFMS can achieve the collection of intestinal tissues under the alternating application of NIR laser irradiation and an external AC magnetic field. The MFMS has the advantages of rapid movement, responsiveness, and precise positioning, especially its ability to provide storage space that can be controlled to be "opened" and "closed". Therefore, the MFMS has potential to become a medical platform for multi-tasking in the digestive system, which will expand the application of micro- and nanomotors in the field of biomedicine.

Author contributions

Junmin Liu and Zhiyuan Huang contributed equally to this work. Conceptualization: Dekai Zhou; data curation, measurements and analysis: Junmin Liu and Zhiyuan Huang; supervision: Dekai Zhou; investigation: Rencheng Zhuang; methodology: Honger Yue and Rencheng Zhuang; writing – original draft preparation: Junmin Liu; writing – review and editing: Xiaocong Chang, Dekai Zhou, and Longqiu Li; project administration: Dekai Zhou; funding acquisition: Xiaocong Chang, Dekai Zhou, and Longqiu Li. All authors have read and agreed to the final version of the manuscript.

Conflicts of interest

There are no conflicts to declare.

Acknowledgements

This work was supported by the National Natural Science Foundation of China (52125505, 52005138, and U20A20297), the Natural Science Foundation of Heilongjiang Province of China (LH2021E061), the Natural Science Foundation of Chongqing of China (CSTB2022NSCQ-MSX0431 and

CSTB2022NSCQ-MSX1295), the Heilongjiang Touyan Team (HITTY-20190036), and the Fundamental Research Funds for the Central Universities (Grant No. HIT. BRET. 2021005 and HIT. NSRIF. 2020033).

References

1 I. Ben-Aharon, H. W. van Laarhoven, E. Fontana, R. Obermannova, M. Nilsson and F. Lordick, *Cancer Discovery*, 2023, **13**, 538–551.
2 M. B. Loughrey and N. A. Shepherd, *Histopathology*, 2015, **66**, 66–77.
3 D. Y. Cheung, J. S. Kim, K. N. Shim and M. G. Choi, *Clin. Endosc.*, 2016, **49**, 21–25.
4 G. Malietzis, O. Aziz, N. M. Bagnall, N. Johns, K. C. Fearon and J. T. Jenkins, *Eur. J. Surg. Oncol.*, 2015, **41**, 186–196.
5 J. Wang and K. M. Manesh, *Small*, 2010, **6**, 338–345.
6 P. L. Venugopalan, S. Jain, S. Shivashankar and A. Ghosh, *Nanoscale*, 2018, **10**, 2327–2332.
7 J. Li, B. Esteban-Fernandez de Avila, W. Gao, L. Zhang and J. Wang, *Sci. Rob.*, 2017, **2**, eaam6431.
8 Z. Wu, B. E. F. De Avila, A. Martín, C. Christianson, W. Gao, S. K. Thamphiwatana, A. Escarpa, Q. He, L. Zhang and J. Wang, *Nanoscale*, 2015, **7**, 13680–13686.
9 F. Peng, Y. Tu and D. A. Wilson, *Chem. Soc. Rev.*, 2017, **46**, 5289–5310.
10 M. Pacheco, B. Jurado-Sánchez and A. Escarpa, *Nanoscale*, 2021, **13**, 17106–17115.
11 M. Sun, X. Fan, X. Meng, J. Song, W. Chen, L. Sun and H. Xie, *Nanoscale*, 2019, **11**, 18382–18392.
12 W. Wang, Z. Wu, X. Lin, T. Si and Q. He, *J. Am. Chem. Soc.*, 2019, **141**, 6601–6608.
13 M. Kwak, I. Jung, Y. G. Kang, D. K. Lee and S. Park, *Nanoscale*, 2018, **10**, 18690–18695.
14 H. Xu, M. Medina-Sánchez, V. Magdanz, L. Schwarz, F. Hebenstreit and O. G. Schmidt, *ACS Nano*, 2018, **12**, 327–337.
15 X. Wei, M. Beltrán-Gastélum, E. Karshalev, B. Esteban-Fernández de ávila, J. Zhou, D. Ran, P. Angsantikul, R. H. Fang, J. Wang and L. Zhang, *Nano Lett.*, 2019, **19**, 1914–1921.
16 W. Chen, X. Chen, M. Yang, S. Li, X. Fan, H. Zhang and H. Xie, *ACS Appl. Mater. Interfaces*, 2021, **13**, 45315–45324.
17 Y. Zhang, L. Zhang, L. Yang, C. I. Vong, K. F. Chan, W. K. Wu, T. N. Kwong, N. W. Lo, M. Ip and S. H. Wong, *Sci. Adv.*, 2019, **5**, eaau9650.
18 A. Chalupniak, E. Morales-Narvaez and A. Merkoci, *Adv. Drug Delivery Rev.*, 2015, **95**, 104–116.
19 B. Khezri, S. M. B. Mousavi, Z. Sofer and M. Pumera, *Nanoscale*, 2019, **11**, 8825–8834.
20 S. Ketzetzi, M. Rinaldin, P. Dröge, J. D. Graaf and D. J. Kraft, *Nat. Commun.*, 2022, **13**, 1772.
21 S. Cao, H. Wu, I. A. Pijpers, J. Shao, L. K. Abdelmohsen, D. S. Williams and J. C. Van Hest, *ACS Nano*, 2021, **15**, 18270–18278.
22 R. Zhuang, D. Zhou, X. Chang, Y. Mo, G. Zhang and L. Li, *Appl. Mater. Today*, 2022, **26**, 101314.
23 L. Zhang, Z. Xiao, X. Chen, J. Chen and W. Wang, *ACS Nano*, 2019, **13**, 8842–8853.
24 T. Xu, L. P. Xu and X. Zhang, *Appl. Mater. Today*, 2017, **9**, 493–503.
25 A. Aghakhani, A. Pena-Francesch, U. Bozuyuk, H. Cetin, P. Wrede and M. Sitti, *Sci. Adv.*, 2022, **8**, eabm5126.
26 T. Xu, W. Gao, L. P. Xu, X. Zhang and S. Wang, *Adv. Mater.*, 2017, **29**, 1603250.
27 Y. Feng, D. Jia, H. Yue, J. Wang, W. Song, L. Li, A. Zhang, S. Li, X. Chang and D. Zhou, *Small*, 2023, **19**, 2207565.
28 X. Peng, M. Urso, J. Balvan, M. Masarik and M. Pumera, *Angew. Chem., Int. Ed.*, 2022, **61**, e202213505.
29 X. Dong, S. Kheiri, Y. Lu, Z. Xu, M. Zhen and X. Liu, *Sci. Rob.*, 2021, **6**, eabe3950.
30 H. Yue, X. Chang, J. Liu, D. Zhou and L. Li, *ACS Appl. Mater. Interfaces*, 2022, **14**, 8743–8752.
31 Z. Xiang, G. Jiang, D. Fan, J. Tian, Z. Hu and Q. Fang, *Nanoscale*, 2020, **12**, 13513–13522.
32 S. Jeon, S. H. Park, E. Kim, J. Y. Kim, S. W. Kim and H. Choi, *Adv. Healthcare Mater.*, 2021, **10**, 2100801.
33 A. Kaiser, A. Snezhko and I. S. Aranson, *Sci. Adv.*, 2017, **3**, e1601469.
34 X. Z. Chen, M. Hoop, F. Mushtaq, E. Siringil, C. Hu, B. J. Nelson and S. Pané, *Appl. Mater. Today*, 2017, **9**, 37–48.
35 C. Liu, T. Xu, L. P. Xu and X. Zhang, *Micromachines*, 2018, **9**, 10.
36 L. Schwarz, D. D. Karnaushenko, F. Hebenstreit, R. Naumann, O. G. Schmidt and M. Medina-Sánchez, *Adv. Sci.*, 2020, **7**, 2000843.
37 S. Tottori, L. Zhang, F. Qiu, K. K. Krawczyk, A. Franco-Obregon and B. J. Nelson, *Adv. Mater.*, 2012, **24**, 811–816.
38 W. Gao, S. Sattayasamitsathit, K. M. Manesh, D. Weihs and J. Wang, *J. Am. Chem. Soc.*, 2010, **132**, 14403–14405.
39 G. Gardi, S. Ceron, W. Wang, K. Petersen and M. Sitti, *Nat. Commun.*, 2022, **13**, 2239.
40 Z. Zheng, H. Wang, L. Dong, Q. Shi, J. Li, T. Sun, Q. Huang and T. Fukuda, *Nat. Commun.*, 2021, **12**, 411.
41 Z. Huang, G. Shao, D. Zhou, X. Deng, J. Qiao and L. Li, *Int. J. Extreme Manuf.*, 2023, **5**, 035501.
42 G. Shao, H. O. T. Ware, J. Huang, R. Hai, L. Li and C. Sun, *Addit. Manuf.*, 2021, **38**, 101834.
43 H. Deng, X. Li, Q. Peng, X. Wang, J. Chen and Y. Li, *Angew. Chem., Int. Ed.*, 2005, **44**, 2782–2785.
44 Y. Nagaoka, H. Morimoto and T. Maekawa, *Phys. Rev. E: Stat., Nonlinear, Soft Matter Phys.*, 2005, **71**, 032502.